catalysts

MDPI

Article

Dibenzothiophene Hydrodesulfurization over P-CoMo on Sol-Gel Alumina Modified by La Addition. Effect of Rare-Earth Content

José Escobar [1,*], María C. Barrera [2], Jaime S. Valente [1], Dora A. Solís-Casados [3], Víctor Santes [4], José E. Terrazas [2] and Benoit A.R. Fouconnier [2]

1 Instituto Mexicano del Petróleo, Eje Central Lázaro Cárdenas 152, San Bartolo Atepehuacan, G.A. Madero, Cd. de México 07730, México; jsanchez@imp.mx
2 Facultad de Ciencias Químicas-Centro de Investigación en Recursos Energéticos y Sustentables, Universidad Veracruzana, Campus Coatzacoalcos, Av. Universidad km. 7.5, Col. Santa Isabel, Coatzacoalcos, Veracruz 96538, México; mcbdgavilan@gmail.com (M.C.B.); eterrazas@uv.mx (J.E.T.); broger@uv.mx (B.A.R.F.)
3 Universidad Autónoma del Estado de México. Centro Conjunto de Investigación en Química Sustentable, km. 14.5 Carretera Toluca-Atlacomulco, Toluca, Estado de México 50200, México; solis_casados@yahoo.com.mx
4 Departamento de Biociencias e Ingeniería, Centro Interdisciplinario de Investigaciones y Estudios en Medio Ambiente y Desarrollo (CIIEMAD), Instituto Politécnico Nacional, Ciudad de México C.P. 07340, México; vsantes@ipn.mx
* Correspondence: jeaguila@imp.mx

Received: 11 March 2019; Accepted: 9 April 2019; Published: 13 April 2019

Abstract: Alumina-lanthana (La at 1, 3, or 5 wt%) supports were prepared by sol-gel from Al alkoxide sol where $La(NO_3)_3$ was added. Annealed (550 °C) xerogels were characterized by N_2 physisorption, thermal analysis (TG-DTA), X-ray diffraction (XRD), scanning electron microscopy- energy dispersive spectroscopy (SEM-EDS), CO_2-adsorption studied in IR region, Raman and ultraviolet-vis (UV-vis) spectroscopies. The texture of amorphous binary matrices of high La dispersion was adequate to applications in catalysts for middle distillates hydrodesulfurization (HDS). Generally, the amount and strength of surface basic sites increased with La content in solids. Mo (at 2.8 at. nm^{-2}) and Co (at Co/(Co+Mo) = 0.3) were deposited over carriers by one-pot simultaneous impregnation in the presence of PO_4^{3-} (P_2O_5/(NiO+MoO_3) = 0.2 mass ratio). Calcined (400 °C) Co-Mo-P impregnated precursors had decreased basicity as to that of corresponding carriers, suggesting strong La-deposited species interaction. As La content in carriers increased Mo=O Raman stretching vibrations shifted to lower wave-numbers (949 to 935 cm^{-1}) suggesting octahedral molybdates coordination change to tetrahedral. Although La at the lowest concentration (1 wt%) enhanced dibenzothiophene, HDS (~38% higher as to the Al_2O_3-supported formulation) desulfurization was significantly diminished at augmented content. Presence of hardly sulfidable tetrahedral Mo originated during impregnation at basic conditions in pores of La-modified carriers seemed to dictate observed behavior. Rare earth content in formulations enhanced selectivity to biphenyl.

Keywords: hydrodesulfurization; $CoMo/Al_2O_3$; basic additive; lanthanum

1. Introduction

Improved catalytic formulations of enhanced properties in hydrodesulfurization (HDS) reactions that allow for compliance with ever stricter environmental regulations on S content in internal combustion engine fuels remains a challenging research field. In this context, one of the most relevant lines of investigation involves preparation of improved catalyst supports, where conventional active

phases used in formulations applied at the industrial hydrotreating scale (sulfided Mo or W promoted by either Co or Ni) could have enhanced properties, including better dispersion and sulfidability or more efficient promoter integration [1–3]. In this regard, the effects of using carriers with augmented surface basicity, as to that of conventionally used alumina, still remains a matter of debate. Some reports have shown that over carriers of increased basicity, by alkaline [4] or alkaline-earth metal [5] species addition, catalysts of enhanced selectivity to desulfurization and limited hydrogenating properties could be obtained. That effect has been attributed to several factors, for instance, decreased surface acidity by basic agent addition [4] or formation of oxidic species (magnesium molybdate and NiO-MgO solid solution, [5]) that resulted after sulfiding in MoS_2 (from $MgMoO_4$, for example) phases of increased slab length and diminished saturation ability. However, decreased activity for organo-S species desulfurization (thiophene) was also observed [4], although in a lower degree, as to that registered for alkenes hydrogenation. Formation of K-decorated and K-intercalated MoS_2 phases supported on SBA-15 mesoporous materials of enhanced activity and selectivity to methanethiol from a H_2S-CH_4 mixture have been recently reported [6]. According to the authors, electron donation from K atoms could enhance the electron density of sulfided Mo species that facilitated formation of increased amounts of Mo-coordinatively unsaturated sites (CUS).

Environmentally friendly lanthanum is a cheap rare earth that has been added to catalyst carriers in order to increase their thermal resistance [7] and surface basicity [8]. For instance, decreased acidity of alumina-La oxides contributed to augmented stability in ethanol conversion, due to diminished coke formation [9]. Also, due to that diminished acidity, corresponding rare-earth-modified Al_2O_3 had enhanced selectivity to ethylene (instead of to carbonaceous species) at high ethanol conversion [10]. Augmented basicity provoked by La addition also resulted in improved activity in a rare-earth-modified Ni/alumina formulation tested in CO_2 methanation, that fact being originated by stronger carbon dioxide adsorption as surface carbonates that acted as so-called reactant reservoirs [11]. Higher stability of La-modified HZSM-5 zeolite catalysts in methyl mercaptan decomposition, as to that of the non-doped material, has been attributed to decreased Brønsted acidity [12].

Regarding lanthanum-containing formulations applied as HDS catalysts carriers, to our best knowledge, the information available is rather scarce [13,14]. Diminished activity in thiophene HDS of sulfided CoMo/alumina catalysts modified by La has been attributed to enhanced proportions of isolated MoO_4^{2-} refractory and less-sulfidable species adsorbed on lanthana domains [14]. From their studies on molybdenum supported on La-modified alumina, Massoth et al. [13] found that strong interaction of rare earth oxidic domains with Al_2O_3 resulted in LaO monolayer dispersion. At high La loadings, however, a second lanthanum oxide layer could be formed right over the first, the latter being partially sulfidable under 10% H_2S/H_2 treatment (400 °C, 2 h). Higher activity, as to that of non-doped alumina-supported sulfided Mo catalysts, in both thiophene conversion and hexene saturation was found for formulations of high-La content (≥ 10 wt%). Different trends in those reactions, as a function of rare-earth concentration in tested formulations, were related to electronic support effects, which affected those reactions in distinctive ways. Also, a diminished proportion of disintegration reactions was observed, decreased cracking being originated by the neutralization of surface acidic sites over alumina, due to the basic agent deposition. Considering those contradictory results, the influence of basic La as a carrier additive on HDS catalyst properties deserves further investigation.

Respecting HDS catalysts' active phases (as opposed to corresponding supports), Chevrel phases ($M_xMo_6S_8$, where M could be La) have been synthesized and tested in HDS reaction schemes [15]. Different to conventional MoS_2-based hydrodesulfurization catalysts, where Mo is in 4^+ oxidation state, in Chevrel phases Mo is in either 2^+ or 2.666^+, depending on the type of second metal M. In general, HDS properties of Chevrel phases are not as good as those of MoS_2-based catalysts, which explains why studies on those species (and particularly on those where La is the second metal) are very scarce.

In this work, lanthana modified-alumina at various rare-earth contents (1, 3, and 5 wt%) is used as CoMo-based HDS catalyst support. Textural, structural, and surface properties of carriers and corresponding impregnated materials, in an oxidic phase, were characterized through various

techniques. Sulfided materials were tested in dibenzothiophene (most representative organo-S species present in middle distillates) hydrodesulfurization, in batch reactor at conditions close to those used in commercial-scale hydrotreaters aimed at diesel fuel production from oil-derived feedstocks. The activity trends found were correlated to physicochemical characteristics of studied catalysts. Some advances from this investigation have been recently reported [16].

2. Results and Discussion

2.1. N_2 Physisorption

N_2 physisorption isotherms (Figure S1) of alumina and La-modified supports (see Section 3.1. *Materials Synthesis* for samples nomenclature) were intermediate between types II and IV, according to IUPAC (International union of pure and applied chemistry) classification [17], suggesting mesoporous materials. All solids had type H1 hysteresis characterizing solids with porous networks of uniform size and shape [17], where capillary condensation started at ~P/P_s = 0.5.

From Table 1, La addition was reflected in slightly increased (~10%) surface area (S_{gBET}) as to that of the pristine alumina carrier. More noticeable improvements were observed in both pore volume (V_p) and average pore diameter, that effect being more evident in materials at a higher rare earth content (in ALa3, 40% and 53% higher, respectively, as to sol-gel alumina). The texture of prepared binary matrices was adequate for carriers of catalysts applied in oil-derived middle distillate hydrotreatment aimed at diesel fuel production [18].

Table 1. Textural properties (as determined by low-temperature N_2 physisorption) of ALaz supports and corresponding CoMo-impregnated oxidic materials.

Sample	S_{gBET} ($m^2\ g^{-1}$)	V_p ($cm^3\ g^{-1}$)	D_p [a] (nm)	S_{gBJHa} ($m^2\ g^{-1}$)	S_{gBJHd} ($m^2\ g^{-1}$)
A	308	0.45	5.9	347	435
ALa1	334	0.55	6.6	403	485
ALa3	335	0.69	8.3	423	504
ALa5	326	0.60	7.3	419	505
CM/A	199	0.43	8.6	240	277
CM/ALa1	135	0.26	7.8	191	240
CM/ALa3	211	0.43	8.2	252	291
CM/ALa5	141	0.41	11.7	268	323

[a] $4 \times V_p \times S_{gBET}{}^{-1}$ [19].

Considering Co-Mo-P oxidic impregnated materials (see corresponding isotherms in Figure S2), CM/A had ~35% lower surface area as to that of the Al_2O_3 carrier, commensurate with non-porous oxidic phase loading (~32%), which suggests well-dispersed deposited phases. On the other hand, La-modified supports had significant textural losses after Co-Mo-P impregnation (~60% diminished S_g in CM/ALa1, as to that of the corresponding carrier), pointing to a partial collapse of the binary support matrix. Strandberg anions (phosphopentamolybdates), present in highly acidic impregnating solutions (see Section 3.1. *Materials synthesis*), could probably be decomposed under basic conditions in the interior of pores of rare earth modified materials (as indeed reported in Section 2.6. *Raman spectroscopy*), releasing $PO_4{}^{3-}$ anions. Due to their strong affinity, lanthanum atoms in the solid matrices could strongly interact with those phosphate anions [20,21] being partially leached from the carriers, thus provoking the mentioned partial porous network destruction. Additionally, it has been reported [14] that, when impregnated through originally acidic solutions (as in our case), Mo could partially extract lanthanum atoms deposited over an alumina matrix, forming defined La molybdate domains. It seemed that particle growth could cause an enhanced average pore size (Table 1, as determined by Gurvich´s law [19]) of impregnated Co-Mo-P materials over La-doped carriers. Others [22] have also found that, during HDS catalysts preparation, impregnating conditions could be crucial in preserving textural

properties of corresponding supports, avoiding then their collapse. Expectably, that fact could be reflected in improved catalytic activity.

Pore size distributions (PSD) were determined through Barrett-Joyner-Halenda (BJH) methodology. In order to determine which PSD profile, obtained from an either adsorption or desorption data branch, better fits the actual ones, corresponding cumulative surface area values were compared to those obtained by the BET (Brunauer-Emett-Teller method, Table 1). Values from adsorption branch data (S_{gBJHa}) were closest to the BET ones as to those obtained from desorption data (S_{gBJHd}). Thus, PSD profiles from the former data were deemed the most suitable in describing the actual porous networks. PSD maxima of La-containing sol-gel carriers shifted to higher diameters as to that of non-modified alumina (~6.6 nm), ALa3 showing the maximum average value (~8.5 nm) (Figure S3a). Considering Co-Mo-P impregnated samples (Figure S3b), the maxima of CM/A and CM/ALa5 profiles shifted to larger diameters, as to those of corresponding supports (from 6.6 to 8.6 nm and from 6.4 to 8.1 nm, respectively). The amount of pores with diameters ≤ 5 nm, in the PSD of all carriers, strongly diminished after Co-Mo-P deposition.

2.2. Thermal Analyses (Thermogravimetric and Differential Thermal Analyses, TG and DTA)

Thermogravimetric (TG) and differential thermal analyses (DTA) profiles of various carriers at different La contents were similar, with just small differences (not shown) in either weight losses (TG) or signal intensity (DTA). For example, corresponding plots for ALa5 are included in Figure 1. From room temperature to 550 °C, weight losses at a more or less constant rate were observed. The first part of the TGA curve (until approximately 140 °C) could be related to the evaporation of physisorbed water and alcohol from the sol-gel technique used during materials synthesis [23] (see Section 3.1. *Materials synthesis*). Further losses until 550 °C could be originated by the elimination of both nitrates (from La salt used) and organic remains from the Al alkoxide utilized. The endothermal signal centered at ~140 °C in the ALa5 DTA profile corresponded to aforementioned evaporation of water, alcohol, and structural hydroxyls. Meanwhile, the exothermal peak, at ~220 °C, could be provoked by NO_3^- anion decomposition [24]. The intensity of this signal increased with La content in mixed formulations. The strong exothermal peak, centered at 277 °C, could be provoked by organic residua (from Al alkoxide) combustion [23]. Due to crystallization phenomena (to any Al_2O_3, LaO or La_2O_3 defined phases), no further signals were observed at more severe treatment conditions. In full agreement with our findings, it has been reported [25] that lanthanum addition during sol-gel alumina synthesis contributes to obtaining highly stable binary matrices delaying crystallization to the gamma phase, with defined La phases detected just after high-temperature (1000 °C) annealing.

2.3. X-ray Difracction (XRD)

Diffractograms of various supports at various compositions (not shown) showed no crystalline phases. The amorphousness of carriers suggested homogeneous materials, where La was both well-integrated and well-dispersed in alumina matrices. In Figure 2, diffractograms of the oxide at the highest La content and the corresponding Co-Mo-P impregnated material are shown. Both patterns did not show any diffraction peak, pointing to either well-dispersed deposited molybdates on the support surface or the presence of disordered amorphous Mo domains, undetectable by the used technique [26].

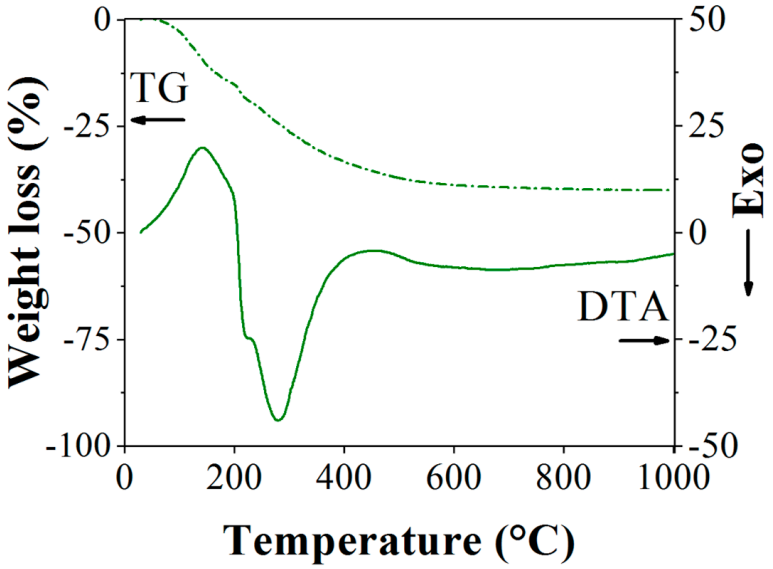

Figure 1. Thermal analysis (TG and DTA) profiles of the ALa5 dried carrier.

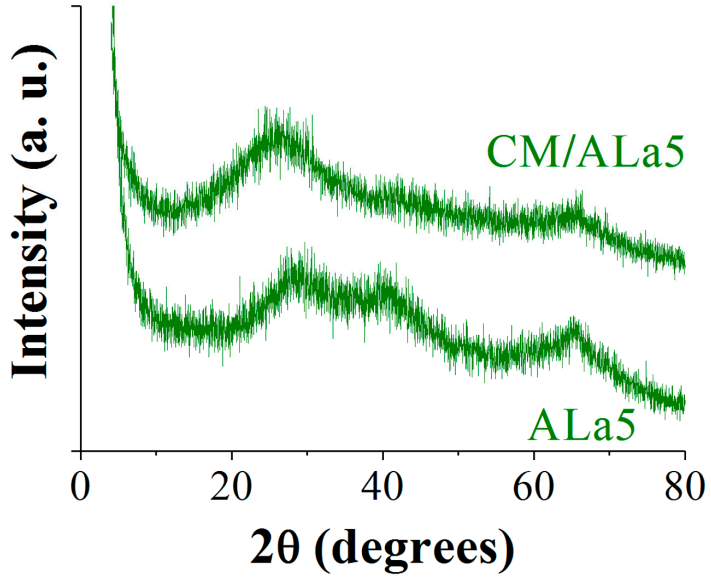

Figure 2. X-ray diffraction patterns of ALa5 support and corresponding P-doped CoMo impregnated oxidic material.

2.4. Chemical Analysis (Scanning Electron Microscopy-Energy Dispersive Spectroscopy (SEM-EDS)

The chemical composition of the supports and the various impregnated materials prepared were determined from EDS (energy dispersive spectroscopy, equipment attached to a SEM, scanning electron microscope, with back-scattered electrons detector). Corresponding micrographs of La-modified carriers and Co-Mo-P impregnated materials are included in Figures S4 and S5, respectively.

No important differences in sample morphology were observed at this stage, all solids being constituted by faceted particles. Regarding Co-Mo-P impregnated solids, morphology of corresponding carriers is preserved (note higher mixrograph magnification in former samples). In Figure 3, representative EDS profiles of samples ALa5 and CM/ALa5 are shown. From Table 2, actual La loading (wt%) in sol-gel carriers nicely corresponded to nominal values, suggesting homogeneous binary matrices.

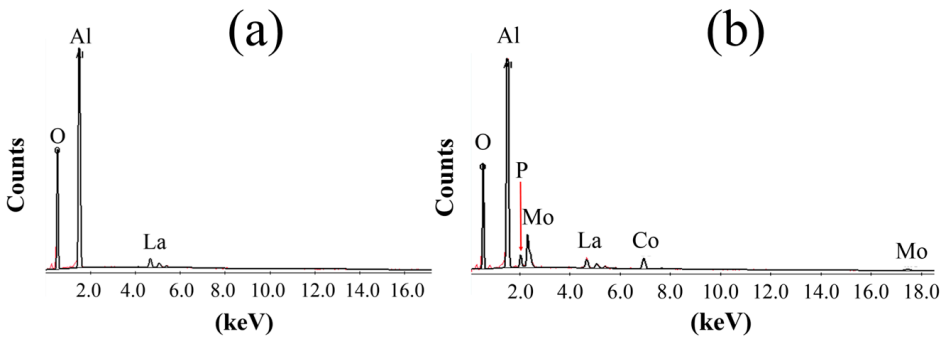

Figure 3. EDS profiles of ALa5 support and corresponding oxidic P-doped CoMo impregnated material. (**a**) ALa5; (**b**) CM/ALa5.

Table 2. Chemical analysis (by SEM-EDS) of La-modified sol-gel alumina supports used.

ALa1	**Wt%**	**At%**
O_K	49.82	63.14
Al_K	48.78	36.66
La_L	1.4	0.2
Total	100	100
ALa3		
O_K	48.55	62.75
Al_K	47.91	36.72
La_L	3.54	0.53
Total	100	100
ALa5		
O_K	48.12	63.15
Al_K	46.27	36.01
La_L	5.6	0.85
Total	100	100

Regarding Co-Mo-P impregnated solids, phosphorus content in CM/A and CM/ALa1 was very similar (Table S1), being slightly lower in the rest of samples. Additionally, Co and Mo contents in samples were alike in all impregnated samples.

2.5. Surface Bascity (CO_2-Adsorption Studied In IR Region, CO_2-FTIR)

The surface basic properties of the studied materials were estimated by integrating the area of peaks registered in the mid-infrared region, between 1800–1200 cm^{-1}, observed after CO_2 room-temperature adsorption [27], followed by thermo-desorption at various temperatures (Table 3). CO_2 has been applied as a probe in determining the density and strength of surface basic sites of La-containing materials [28,29]. Different surface species could be originated by carbon dioxide adsorption, namely, unidentate and bidentate carbonates and bicarbonates [30] (Scheme S1). Carbonates, related to CO_2 adsorbed on surface sites with intermediate and high basic strengths, respectively, requires of surface basic oxygen atoms [31]. Unidentate carbonates, characterized by symmetric and asymmetric O-C-O stretching at 1360–1400 cm^{-1} and 1510–1560 cm^{-1}, respectively, could be originated on isolated low-coordination surface O^{2-} anions in corners or edges. On the other hand, bidentate carbonates that could be formed on Lewis acid-base pairs (M-O^{2-} pair site, where M is La or Al cation, Scheme S1) are characterized by absorptions due to symmetric and asymmetric O-C-O stretching at 1320–1340 cm^{-1} and 1610–1630 cm^{-1}, respectively [31]. Finally, bicarbonates involve CO_2 adsorption on low-strength basic surface hydroxyls [31], showing a C-OH bending mode at 1220 cm^{-1} and symmetric and asymmetric O-C-O stretching vibrations at 1480 cm^{-1} and 1650 cm^{-1}, respectively (Scheme S1). We arbitrarily classified the strength of various types of sites according to the temperature at which they could retain CO_2 (T_d as weak (200 °C < T_d), medium (200 °C > T_d < 400 °C) and strong (T_d > 400 °C).

Table 3. Relative surface basicity (CO_2-FTIR, integrated area of peaks in the 1200–1800 cm^{-1} region) of supports used and corresponding Co-Mo-P oxidic impregnated materials. T_d: Desorption temperature. ND: Non-determined.

T_d (°C)	A	ALa1	ALa3	ALa5	CM/A	CM/ALa1	CM/ALa3	CM/ALa5
25	71	79	96	108	36	30	42	41
100	21	32	54	38	27	16	34	31
200	15	26	44	29	22	7	24	24
300	14	26	42	29	19	6	22	21
400	12	26	41	27	15	5	20	21
500	11	17	33	25	0	ND	13	12

The number of surface basic sites of alumina augmented, by La addition, being that especially evident in samples of higher rare-earth concentration (see, for instance, values from room temperature spectra of ALa3 and ALa5, Table 3). Cui et al. [13] found a linear relationship between the amount of adsorbed CO_2 and La content (until ~20 wt%) in sulfided Mo/alumina samples prepared by rare-earth nitrate impregnation, although non-doped Mo/Al_2O_3 had some surface basicity. In addition, the strength of sites as a function of CO_2, retained after a progressively increased desorption temperature, was clearly enhanced in aforementioned solids. Most of the sites on sol-gel alumina, ALa1 and ALa5, were weak, mainly forming bicarbonates. In the opposite, ALa3 contained the strongest surface basic sites (those related to unidentate carbonates formation) among the studied materials, preserving around the third part of the total number of sites retaining CO_2 at room temperature and after treatment at 500 °C. Additionally, the relative amount of strong sites was three-fold to those over pristine alumina. In full agreement, it has been reported [32] that, on La-modified Al_2O_3 at contents close to monolayer (~5.12 at. La^{3+} nm^{-2} [33]) population of strong sites retaining CO_2, was significantly enhanced.

For Co-Mo-P impregnated samples, the amount of adsorbed CO_2 was clearly diminished as to those of corresponding carriers, with the sole exception of the alumina-supported solid. In this case, significantly decreased basicity (~50%) was registered just in the case of weak sites, which could be related to the well-known strong interaction between molybdate anions and the most basic hydroxyl groups on Al_2O_3 surface [34] (those related to bicarbonates formation during CO_2 adsorption experiments). Additionally, CM/ALa1 lost around 62% of sites adsorbing CO_2 at room temperature. The observed trend was even more marked regarding strong sites (~80% loss). Those facts could probably be related to strong deposited phases-La interaction. In the opposite, CM/ALa5 retained between 72%–83% of medium strength sites (mainly related to bidentate carbonates) of those on corresponding support. Due to strong Co [35], Mo [14] and P [20,21] interaction with La, it is probable that after impregnation the rare-earth could be lixiviated, to some extent, from the sol-gel matrix, with that fact explaining the partial textural collapse (Table 1). According to Cui et al. [13], during impregnation, Mo could preferably interact with La domains then with the alumina carrier. In addition, Ledford et al. [35] found that, in materials of La/Al ≥ 0.0075 atomic ratio (as in the case of our carriers with 3 and 5 wt% La), a Co-La phase could be formed that, being reflected in, lessened cobalt reducibility. The effects of lanthanum extraction could be more significant in the sample of the lowest rare earth content (CM/ALa1), rationalizing the important surface basicity lost. Conversely, the Co-Mo-P impregnated samples of enhanced La concentration had around 33% more sites retaining CO_2 at 400 °C as to the alumina-supported solid, pointing out the retention of mid-strength basic sites.

2.6. Raman Spectroscopy

Al_2O_3 does not show any Raman band due to the low polarizability of light atoms and the ionic character of Al-O bonds [36]. Characteristic peaks of lanthana at 104, 191 [37], 310, 350, and 415 cm^{-1} [38] were not evidenced, pointing to the absence of La_2O_3 definite domains in our oxidic carriers. Raman signals at 225, 359, 911 (shoulder), and 949 cm^{-1} were observed in the CM/A spectrum

(Figure 4a). The former two signals could be assigned to Mo-O-Mo and O-Mo-O vibrations [39]. Meanwhile, those at higher wavenumbers were related to Mo=O bands. They were ascribed to Anderson species $Al(OH)_6Mo_6O_{18}^{3-}$ [40], whose presence suggested partial support dissolution during contact with the acidic Co-Mo-P impregnating solution (pH ~2.5). Considering the Mo/P ratio in those solutions (~2.0) and their pH, $H_2P_2Mo_5O_{23}^{4-}$ anions (two PO_4 tetrahedrons surrounded by five interconnected octahedral MoO_6 species) could, very probably, be preferentially present [40,41]. Although, due to their stability, those Strandberg heteropolyanions ($H_xP_2Mo_5O_{23}^{(6-x)-}$) [42] could exist in various protonation states over a wide pH range [41], they could be decomposed to phosphates and molybdates owing to their strong interaction with both basic hydroxyls and Al^{3+} coordinatively unsaturated (CUS) Lewis acid sites on alumina surfaces [43].

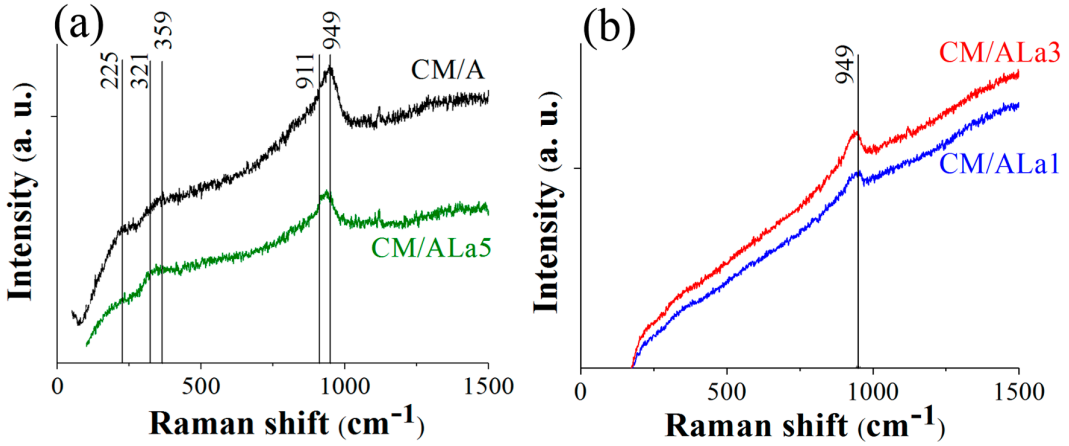

Figure 4. Raman spectra of oxidic Co-Mo-P impregnated materials. (**a**) CM/A and CM/ALa5; (**b**) CM/ALa1 and CM/ALa3.

In spite of some fluorescence interference that decreased sensitivity of the technique used, CM/ALa1 and CM/ALa3, Raman spectra (Figure 4b) evidenced that the signal related to M=O stretching vibrations progressively shifted to a lower wavelength as the rare earth concentration increased, being registered at 935 cm^{-1} for CM/ALa5 (as compared to 949 cm^{-1} observed in CM/A spectrum, Figure 4a). That fact, accompanied by the apparition of a signal at 321 cm^{-1} (more evident in CM/ALa5), strongly suggested the co-existence of both octahedral and tetrahedral Mo species in La-containing samples. In full agreement, Payen et al. [14] reported that the Mo/ La ratio determined the type of oxomolybdenum entities adsorbed on lanthanum-modified alumina. Monomeric tetrahedral species (MoO_4^{2-}) could be preferably formed by an interaction with La-OH groups, whereas polymeric octahedral molybdates could be deposited on Al_2O_3 domains. For materials at a high La concentration (Mo/La~1), just tetrahedral molybdates were observed [14]. In the same line, tetrahedral Mo species were mainly found [44] on basic magnesium-modified sol-gel alumina supports. It seemed that the high point of zero charge values of carriers with basic properties determined that behavior, as in contact with water those solids could produce high pH impregnating conditions where MoO_4^{2-} species are favored. Additionally, coordination state modifications of Mo^{6+} species, from octahedral to tetrahedral (as determined by corresponding Raman shifts), by basic additive doping of alumina-supported unpromoted Mo (Mg, [5]) and CoMo formulations have been reported by others (K [45], Mg-Li [46]).

Definite domains (although not large enough to be detectable by X-ray diffraction) of lanthanum molybdate have also been registered [14] by impregnating La-modified alumina with acidic solutions prepared from ammonium heptamolybdate. In our case, contributions of characteristic bands at 915 and 940 cm^{-1} could not be discarded, although, due to the low intensity of the registered peaks, they could remain masked. If existent, $La_2(Mo_4)_3$-like domains could also be responsible for tetrahedral molybdenum presence [47]. According to the peaks' intensity in spectra, in Figure 4a,b, it seemed that samples CM/ALa1 and CM/ALa5 were the ones with the highest Mo dispersion (although with a high

proportion of tetrahedral species). Small signals, at 1119 cm^{-1}, could be related to C-C bond stretching vibrations [48], probably originated by organic remains from either aluminum alkoxide used during carrier synthesis or due to acetate utilized during Co impregnation.

2.7. UV-Vis Spectroscopy

Being an insulator alumina does not absorb in ultraviolet-visible (UV-vis) region [49]. Absorptions in the 267–306 nm range (more notable for ALa1, Figure 5) could be related to charge transfer from O^{2-} to framework La^{3+} ions [50]. Regarding Co-Mo-P impregnated materials, the O^{-2} →Mo^{6+} charge transfer transition bands of tetrahedral ($Mo_{(Th)}{}^{6+}$) and octahedral ($Mo_{(Oh)}{}^{6+}$) molybdenum species were centered at ~280 and ~314 nm, respectively [51] (Figure 6). That fact suggests that, although basic pH conditions that prevailed during Co-Mo-P impregnation of rare-earth-containing carriers strongly contributed to formation of isolated monomeric $Mo_{(Th)}{}^{6+}$ species (Figure 4a,b), $Mo_{(Oh)}{}^{6+}$ species co-existed with them, as already suggested by our Raman spectroscopy studies (Section 2.6). As proposed by Payen et al. [14], $Mo_{(Th)}{}^{6+}$ species, related to molybdenum in strong interaction with the support, could be related to La domains, whereas $Mo_{(Oh)}{}^{6+}$ ones could be deposited on alumina surfaces. As the former species were absent in the impregnating solutions (containing octahedral Mo^{6+} heteropolyanions) their presence strongly pointed to the decomposition of the Strandberg species through their interaction with basic OH groups and CUS (Lewis sites) on the Al_2O_3 carrier surface [43]. As aforementioned, basic conditions prevalent in the pores of La-modified carriers could also play a major role in tetrahedral Mo^{6+} species formation. The bathochromic shift of the $Mo_{(Oh)}{}^{6+}$ low-energy absorption edge strongly suggested an augmented oxomolybdates polymerization degree [52] in La-containing formulations as to that in CM/A following the order: CM/ALa1 > CM/ALa3 > CM/ALa5 > CM/A. The diminished surface area of lanthanum-modified CM materials (Table 1) could contribute to lowered octahedral Mo species dispersion. Indeed, a shoulder at ~370 nm, whose intensity increased according to the order CM/ALa1 > CM/ALa3 > CM/ALa5, pointed to the formation of MoO_3 domains [53].

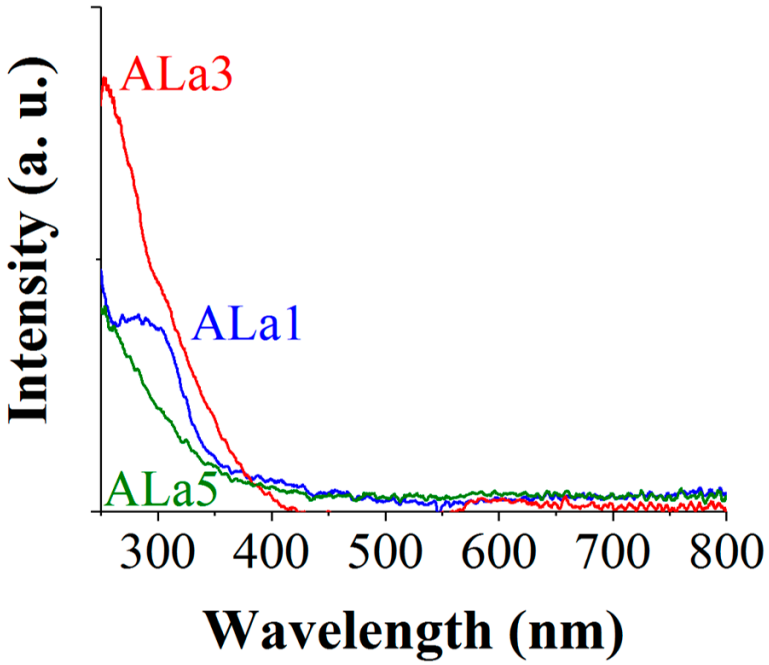

Figure 5. UV-vis spectra of La-modified alumina supports.

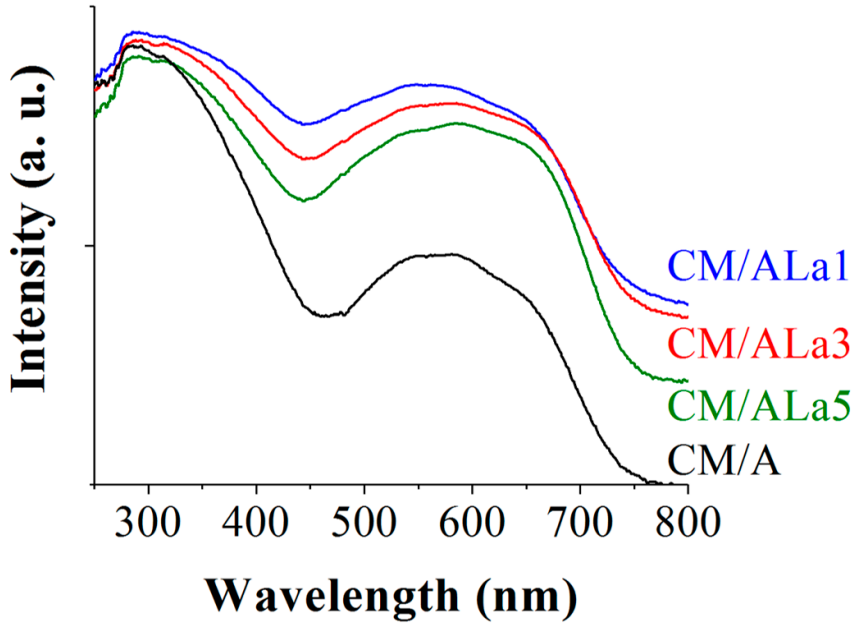

Figure 6. UV-vis spectra of Co-Mo-P impregnated oxidic formulations on La-modified Al_2O_3. Alumina-supported material included as reference.

The triplet band related to $^4A_2(F) \rightarrow {}^4T_1(P)$ transitions of tetrahedral cobalt $Co_{(Td)}{}^{2+}$ at 540, 580, and 625 nm [51] was augmented in rare earth-modified solids, but with no definite trend regarding La concentration. Those cobalt species could be originated in lanthanum cobaltate-like entities. Interestingly, the enhanced proportion of tetrahedral Co^{2+} in alumina-supported CoMo oxidic formulations has been observed in the past by progressively increasing the basic additives concentration (Mg and Li) [46], with augmented $CoAl_2O_4$ formation being invoked in that case. For La-containing samples, shoulders at ~495 and ~563 nm could be related to octahedral Co^{2+} species cobalt ($Co_{(Oh)}{}^{2+}$) [54]. These signals progressively increased in the order CM/ALa1 > CM/ALa3 > CM/ALa5, being essentially absent in the alumina-supported formulation. Additionally, a small shoulder at 518 nm (probably from $^4T_{1g}(F) \rightarrow {}^4T_1g(P)$ electronic transition) suggested $Co_{(Oh)}{}^{2+}$ entities [55] in the CM/ALa1 spectrum.

2.8. HDS Reaction Test

La content in supports of sulfided Co-Mo-P (see 3.3. HDS Reaction Test) catalysts clearly affected their dibenzothiophene HDS activity (Figure 7). The formulation with the lowest rare-earth content had the highest pseudo first order kinetic constant value (~38% enhanced as to that of the non-doped Al_2O_3-supported material). However, significant diminution in HDS properties was observed as lanthanum concentration augmented in tested materials. Payen et al. [14] reported progressive diminution in thiophene HDS activity as La content in alumina- supported CoMo formulations increased. Very probably, enhanced proportions of refractory tetrahedral $MoO_4{}^{2-}$ (see Section 2.6. *Raman spectroscopy*), as rare earth content in formulations augmented, could be primarily responsible for that behavior. Those species are characterized by being hardly sulfidable under the used conditions [14], then precluding MoS_2 phase formation.

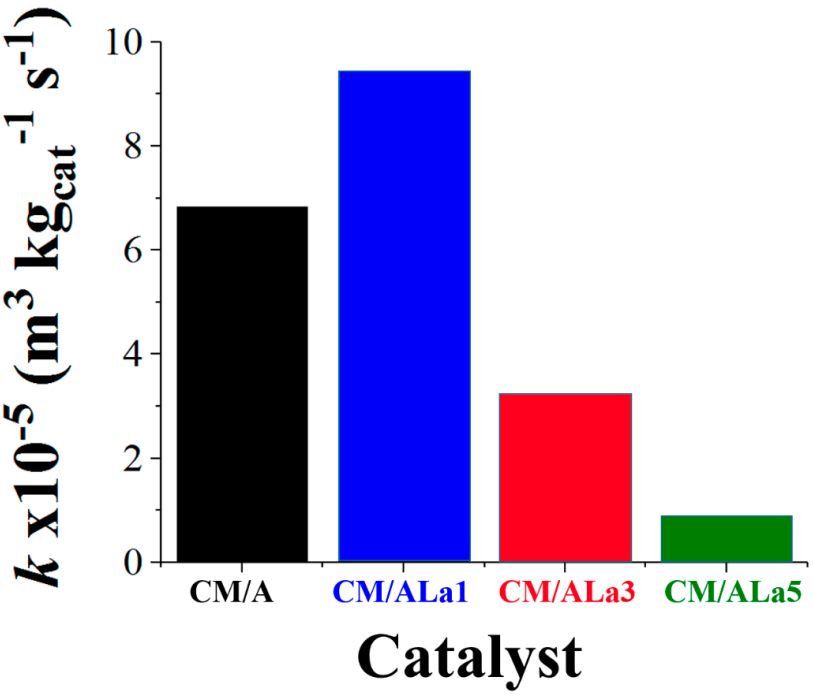

Figure 7. Pseudo first order kinetic constant (DBT HDS) of various tested catalysts. Batch reactor, *n*-hexadecane as solvent, P = 5.67 MPa, T = 320 °C, 107 rad s^{-1} (1030 rpm) mixing speed.

The increased amount of MoO_4^{2-} species by the addition of basic agents in alumina-supported HDS catalysts has been reported in the past [14,56]. For instance, Malet et al. [56] found augmented proportions of hardly-reducible tetrahedral molybdenum entities in Mo/TiO_2 solids doped with Na (through NaOH impregnation) at various concentrations. The decreased reducibility of tetrahedral Mo^{6+} species on Al_2O_3-supported oxidic Mo and CoMo formulations modified by basic agents (Mg and Li) was confirmed by temperature-programmed reduction studies [5,46]. Regarding sulfided alumina-supported CoMo formulations modified by K addition (2.7 wt%), Maugé et al. [4] observed (by FTIR) decreased intensity in bands related to adsorbed CO as to that over the counterpart with a non-doped Al_2O_3 carrier. That could mean a lower proportion of sulfided phases, although the authors mainly attributed that to adsorption sites poisoning provoked by augmented sulfided phase electron density that could be reflected in diminished CO adsorption strength, under tested conditions (−173 °C). Similar to our case, those authors identified enhanced surface basicity of K-doped solids by formation of hydrogen carbonates and bidentate carbonates (weak and medium strength sites, respectively [30]), as studied by CO_2 adsorption followed by FTIR). Decreased conversion in the 2-methylthiophene in *n*-heptane was observed in the case of K-doped CoMo/alumina catalysts when tested in a model FCC (fluid catalytic cracking) naphtha mixture also containing 2,3-dimethylbut-2-ene and orthoxylene. Regarding unpromoted sulfided alumina-supported Mo catalysts, Cui et al. [13] observed unaltered activity in thiophene HDS for materials at low La content (2 wt%), which was followed by decreased desulfurating properties in the solid modified with 5 wt% rare earth loading. Regarding the effect of basic additives on dibenzothiophene (DBT) HDS activity of alumina-supported materials, strongly decreased activity was observed [44] in the case of NiMo formulations with a MgO-modified (5 mol%) Al_2O_3 carrier. As the HDS activity of sulfided Mo has often been related to surface acidity [57], it seems reasonable to assume that diminished Brønsted or Lewis ones (or both) in formulations doped with basic additives could provoke limited organo-S species conversion.

The high activity in DBT HDS of our sulfided alumina-supported Co-Mo-P formulation modified with lanthanum at the lowest content could result from a combination of factors. Our UV-vis results (Figure 6) suggested that, in CM/ALa1, extant octahedral molybdenum species were at lower interaction with the support. Although, according to Raman characterization (Figure 4), amount of refractory

tetrahedral Mo entities augmented in that formulation, as to those over the non-doped material with an Al_2O_3 carrier, the proportion of those monomeric species seemed to be not large enough to significantly affect proportion of sulfidable phases. In addition, the increased proportion of octahedral Co^{2+} (as also observed by UV-vis, Figure 6) in the corresponding oxidic solid could be beneficial as that species is considered a precursor of cobalt that could efficiently form the highly active "CoMoS" phase during catalyst activation by sulfiding (see Section 3.3. *HDS Reaction Test*) [58]. A linear relationship between $Co_{(Oh)}{}^{2+}$ concentration in oxidic materials and HDS activity, in both gas-phase thiophene conversion and liquid phase real feedstock (vacuum gas oil and deasphalted oil) desulfurization, was found in that case. Interestingly, improved DBT HDS activity (as to that of corresponding non-modified catalysts) was observed in CoMo/alumina modified by basic agent addition, but just at a low doping agent content (1.2 wt% Mg or that solid with additional 4 wt% potassium loading) [59]. However, and similarly to our case, HDS activity significantly diminished by augmenting basic species concentration in corresponding sulfided catalysts. Additionally, Cao et al. [60] reported decreased DBT HDS activity on magnesium modified (20 wt% MgO) CoMo/Al_2O_3 materials.

Very interestingly, it has been reported [61] that activity in the SO_2 conversion to sulfur, using coal gas as a reductant, of La-modified sulfided (at similar conditions to those used in the present work, Section 3.3. *HDS Reaction Test*) Co-Cu/γ-Al_2O_3 catalysts was significantly improved over formulations at low rare earth content, as to that of the reference non-doped formulation. Activity was augmented by adding 0.5 wt% rare earth, the maximum being found at 1 wt% La. However, diminished SO_2 conversion was observed by augmenting dopant concentration (4 wt%). The authors attributed that to excessive La_2O_3 loading that could accumulate around crystals of active components, generating an undesired phase change by embedding corresponding particles. Those facts clearly show that La-modified sulfided catalysts at low rare-earth contents deserve further studies, not just in HDS reaction schemes. It is also worth mentioning that recently [62] we reported on the increased activity in naphthalene conversion of Pt (1 wt%) supported on alumina modified with a basic additive (Mg in this case) at low content, as compared to the non-doped formulation with the Al_2O_3 carrier. However, and similarly to what found during the present investigation, activity diminished in materials with a higher magnesium content (8 wt%).

Regarding selectivity to various products, DBT conversion could be carried out through direct desulfurization (DDS, to biphenyl, BP) and hydrogenation (HYD, firstly to hydrodibenzothiophenes, HDBT's) [63] reaction pathways (Scheme S2). At our reaction conditions (see Section 3.3. *HDS Reaction Test*), bicyclohexyl (BCH) saturation, from both aromatic rings, was observed just in trace amounts. Taking into account that BP hydrogenation to cyclohexylbenzene (CHB) could be strongly inhibited by DBT competitive adsorption under our HDS conditions, all CHB produced must have predominantly come from the HYD route through the sulfur removal of partially saturated HDBTs [64]. Selectivity to BP was clearly enhanced with La content in sulfided formulations at isoconversion (x ~17%) (Figure 8). Previous studies in HDS of DBT [65,66] and benzothiophene (BT) [67] strongly evidenced that an augmented DDS/HYD ratio could be related to more efficient MoS_2 promotion by proper Co integration, then enhanced "CoMoS" phase formation. In this direction, Kaluža et al. [67] proposed that the amount of dihydrobenzothiophene (DHBT, formed from BT aromatic ring partial saturation) that could be then subsequently eliminated by C-S hydrogenolysis could be a measure of relative hydrogenation/hydrogenolysis selectivity. During their studies on CoMo sulfided formulations with various carriers, it was found that a very high promotion degree (17.9, over MgO-supported catalyst) was accompanied by a significantly decreased DHBT formation.

In the case of CoMo materials supported on alumina modified by basic agents, significantly augmented DDS/HYD selectivity in DBT HDS has been reported [46] in the past. For instance, by adding magnesia (0.05 mol ratio) to an Al_2O_3 carrier CoMo catalysts producing strongly increased (100% enhancement at 30% conversion) DDS/HYD ratio were obtained. Even more, selectivity to biphenyl was further progressively augmented by additional lithium doping of the aforementioned

formulation. Others [44] have also found decreased DBT transformation through the HYD route over sulfided NiMo catalysts supported on alumina modified by 5 mol% magnesia.

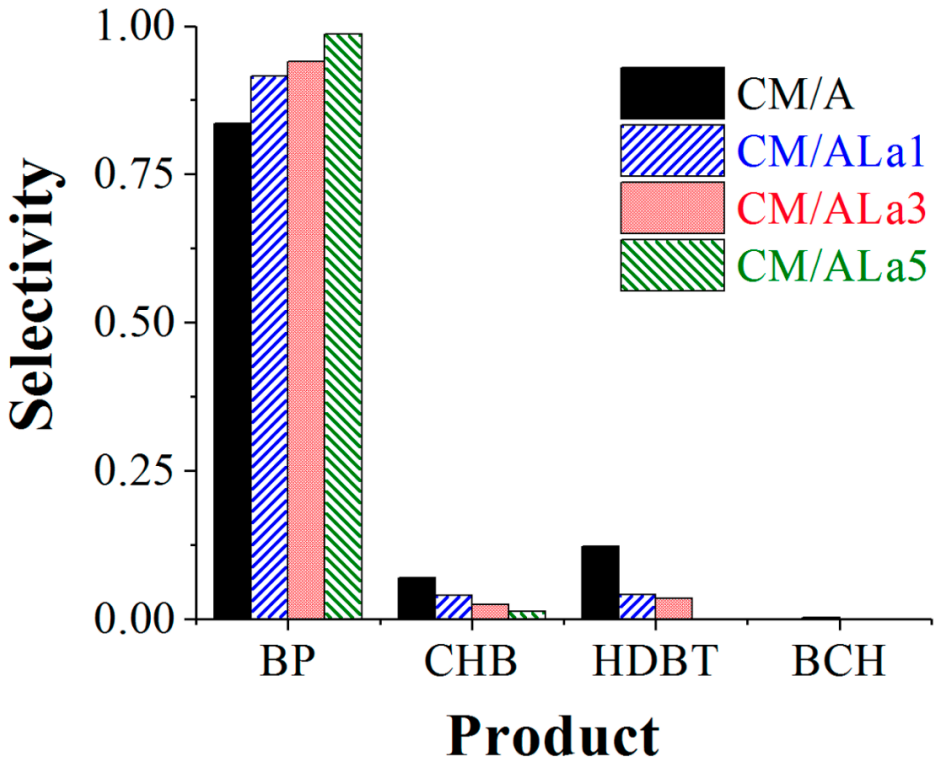

Figure 8. Selectivity to various products (DBT HDS, ~17% conversion), of various tested catalysts. HDBT: hydrodibenzothiophenes; BP: biphenyl; CHB: cyclohexylbenzene; BCH: bicyclohexyl. Batch reactor, *n*-hexadecane as solvent, P = 5.67 MPa, T = 320 °C, 107 rad s^{-1} (1030 rpm) mixing speed.

Following this line of reasoning, the enhanced DDS/HYD ratio, in our case, could be originated by well-promoted (by Co) MoS_2 slab edges, whose number could be restricted due to limited Mo^{6+} sulfidation provoked by extant tetrahedral species. That could justify low DBT HDS activity of formulations of higher La content where cobalt could yet be properly integrated to molybdenum sulfide edges. In those catalysts, however, a certain proportion of the sulfided promoter could be as partially segregated Co_xS_y domains (of marginal HDS activity [66]) due to the reduced number of MoS_2 layer edges, where they could be properly incorporated to produce the highly active "CoMoS phase".

Well-dispersed molybdenum sulfide phases (thus composed of short slabs) could be very efficient in aromatic ring hydrogenation [68]. HYD sites have been related [46] to corner sites in Co-MoS_2 slabs, whose proportion decreases as slab length grows. Those longer molybdenum sulfide layers could be originated by oxidic molybdates of lower dispersion, similarly to that proposed by Halachev et al. [69] in the case of alumina-supported P-modified NiW materials where the ratio W=O/W-O-W, considered as a measure of dispersion of oxidic tungsten species, was related to naphthalene hydrogenation activity of corresponding sulfided formulations. Solids with a higher proportion of terminal M=O bonds resulted (after sulfiding) in catalysts with improved dispersion, and, thus, with enhanced saturation properties. In the opposite, materials with diminished dispersion resulted in decreased hydrogenating capabilities by generating longer MoS_2 with an increased edge sites/corner sites ratio. In this regard, it should be mentioned that, in our case, La-addition resulted in materials with lower oxidic Mo^{6+} phases dispersion (Figure 6). Interestingly, sulfided CoMo/alumina catalysts with limited dispersion (longer slabs and augmented stacking) have also shown [70] enhanced HDS of thiophenic species, accompanied by decreased olefins hydrogenation in the selective hydrotreating of FCC naphtha focused on lowering octane number losses.

Bataille et al. [65] proposed that the main role of the promoter in DBT HDS is to enhance the reaction rate through the DDS pathway, or the C-S bond breakage activity in general. The involved mechanism could consist of attacking a hydrogen atom, in a β position relative to the S atom in a DBT molecule, by a basic sulfur anion. Primarily, both reaction routes (DDS and HYD) require a dihydrodibenzohiophene intermediate [65]. Cleaving the C-S bond to produce two phenyl rings species (BP) could be carried out by hydrogenating one of the double bonds (in any of the aromatic rings) in the sulfur atom vicinity, resulting in the dihydrogenated DBT. Then, the C-S bond in the partially saturated ring could be opened by an elimination process. The second C-S bond cleavage, leading to BP, could possibly occur through a similar mechanism [65].

As the promoter (either Ni or Co) increases electron density of basic S anions, they could favor C-S bonds cleavage. The possibility of electron-rich alumina-lanthana supports contributing to increased sulfur anion basicity (then enhancing the DDS reaction pathway), as recently reported in the case of K-doped MoS_2 phases applied in methanethiol synthesis from a H_2S-CH_4 mixture [6], remains a question that deserves to be answered. Mechanistic studies on DBT HDS over La-modified alumina supports are clearly needed, as information on reaction routes and kinetic parameters could provide valuable parameters that could be useful in investigations focused on applying that kind of catalyst under more realistic conditions in the presence of oil-derived middle distillates [71].

Regarding CoMo alumina formulations modified by La at various loadings, Payen et al. [14] found a similar promotion degree in the thiophene HDS as to that observed over a non-modified solid with an Al_2O_3 carrier. Different trends, as to those reported by others, for corresponding catalysts doped with basic agents (in BT HDS, for instance [67]) could be originated in distinctive rate-limiting steps in tested reactions. Unfortunately, no data on selectivity through DDS and HYD reaction pathways were provided in that case [14].

From the results of the present investigation we consider that sulfided CoMo formulations, supported on alumina doped with La at low concentration (up to 1 wt%), clearly deserve deeper studies. These ongoing investigations will be the subject of further reports.

Finally, the development of HDS catalysts with enhanced activity and increased DDS/HYD selectivity ratio (as our CM/ALa1 formulation) results is promising considering their limited consumption of expensive hydrogen, mainly in the case of H_2-constrained refineries.

3. Experimental

3.1. Materials Synthesis

Al_2O_3-La_2O_3 mixed oxides at three compositions (1, 3, and 5 wt%, ALa1, ALa3, and ALa5, respectively) were prepared by a sol-gel method. First, aluminum alkoxide was dissolved at 80 °C in corresponding alcohol (ROH/alkoxide = 60), under stirring and refluxing being kept during 2 h. Then, water and HNO_3 (3 N) hydrolysis catalysts [23] were added (H_2O/alkoxide= 1, HNO_3/alkoxide = 0.03, respectively), the mixture being kept under stirring and refluxing during approximately 1 more h until sol formation. Pertinent amounts of $La(NO_3)_3{\cdot}6H_2O$ in an alcoholic solution were added to the prepared alumina sol. Additional amounts of distillated water were supplied until total aluminum alkoxide hydrolysis. The mixtures were kept under stirring and reflux during 1 more h at room temperature until gelification. The obtained gels were aged, dried (~100 °C), and further calcined (550 °C, 4 h).

Over annealed mixed oxides Mo and Co were deposited (at 2.8 atoms Mo nm^{-2} and (Co/(Co+Mo)) = 0.3, respectively). Pore-filling simultaneous impregnation was carried out over previously dried supports (120 °C, 2 h) with an acidic solution (pH ~2.5) prepared from digestion (at ~80 °C, in water and under vigorous stirring, 4 h) of MoO_3 99.5 wt% (PQM) in the presence of H_3PO_4 85.3 wt% (Tecsiquim, Mexico City, Mexico). H_2O in excess (typically 250 ml of starting solution to impregnate 5 g of carrier) was used to accelerate molybdenum salt dissolution and digestion. A yellow transparent solution was obtained after hydrolysis. $(CH_3COO)_2Ni{\cdot}4H_2O$ (Sigma-Aldrich, Darmstadt, Germany) was then added, with the stirring and processing temperature being maintained for 2 h. A P_2O_5/(NiO+MoO_3) = 0.2 mass

ratio was fulfilled [72]. A transparent dark wine solution was thus finally obtained. The solution volume was then reduced by evaporation until reaching the suitable one for pore-filling impregnation of the given mass of support. The described one-pot impregnation method was chosen as it constitutes a readily scalable methodology during catalyst preparation at the commercial scale. After impregnation materials were left aging overnight at room temperature for the diffusion of the impregnated species into the carrier porous network. Then, the materials were dried (2 h at 120 °C) and further calcined (400 °C for 5 h). Impregnated solids were identified by using the CM/ALa*z* key, where "*z*" represents La loading in corresponding supports.

3.2. Materials Characterization

Textural properties of prepared materials were determined by N_2 physisorption (at −198 °C, nitrogen saturation temperature at Mexico City barometric pressure) in a Micromeritics (Norcross, GA, USA) ASAP 2000 apparatus after ultra-high vacuum (133.32×10^{-5} Pa) degassing at 300 °C for 2 h to eliminate adsorbed molecules. The surface area (BET, Brunauer-Emett-Teller method), pore volume, and average pore size of the materials (BJH, Barrett-Joyner-Halenda method) were determined from the corresponding isotherms.

Thermal analyses (thermogravimetric and differential thermal analysis (TG and DTA, respectively) of dried (non-calcined) samples were carried out with a Netzsch Thermische Analyze (Burlington, MA, USA) STA 409 EP apparatus, under a static air atmosphere. The crystallographic order of the studied samples was determined by powder X-ray diffraction (XRD, Siemens (Munich, Germany) D-500 Kristalloflex, copper anode, $Cu_{K\alpha}$ radiation, $\lambda = 0.15406$ nm, 35 kV, 25 mA), in the 5–80° 2θ range.

Scanning electron microscopy pictures and chemical analysis by energy dispersive spectroscopy (EDS) of the prepared samples were performed in an environmental scanning electron microscope XL30 with an attached energy dispersive X-ray spectroscope (EDAX, Berwyn, PA, USA).

The surface basicity of alumina, alumina-lanthana supports, and the corresponding impregnated materials were characterized by CO_2 adsorption studied in the mid-infrared region. As an acid probe, carbon dioxide interacts with basic catalysts' surfaces, forming bidentate carbonates, unidentate carbonates, and bicarbonates (Scheme S1, [30]), depending on surface basic site strength. Previously, to corresponding studies, all materials (carefully weighed) were submitted to thermal treatments (500 °C), under an inert atmosphere, to eliminate adsorbed species. Samples were cooled down to room temperature with CO_2 being then fed to the system (at room temperature). Once samples were saturated, the flow of probe gas was suspended, with excess CO_2 being flushed by an inert gas stream. The corresponding spectra were acquired by using a Nicolet (Waltham, MA, USA) Magna 560 FTIR spectrometer at 4 cm^{-1} resolution (50 scans) in diffuse reflectance mode. The analyzed samples were treated at various progressively higher temperatures (25–500 °C) and detected peaks in the 1800–1200 cm^{-1} wavenumbers infrared range (corresponding to formed surface bicarbonates and carbonates) were then registered and integrated.

The Raman spectra of various impregnated samples were obtained using a Jobin Yvon Horiba (Northampton, UK) T64000 spectrometer, equipped with a CCD camera detector. As an excitation source, the 514.5 nm line of a Spectra Physics 2018 Argon/Krypton ion laser system was focused through an Olympus (Tokyo, Japan) BX41 microscope equipped with a 100× magnification objective. Laser power on the sample never exceeded 5 mW to avoid thermal effects on the samples studied.

3.3. HDS Reaction Test

Prepared catalysts were tested in sulfided form (see below) by using a batch reactor, as the main goal was to determine the effect of La content on the HDS properties of otherwise conventional P-modified $CoMo/Al_2O_3$ catalysts. That approach allowed a simple, rapid comparison among the catalytic activity of various studied materials [44,46], although commercial-scale HDS applications in refineries are carried out in fixed-bed plug-flow reactors. Sulfided catalysts were obtained by submitting impregnated precursors to treatment at 400 °C (heating rate 6 °C min^{-1}), under H_2/H_2S (Praxair, Mexico

City, Mexico) flow at 50/6 (ml min^{-1})/(ml min^{-1}) during 2 h. The HDS activity of sulfided catalysts was studied in a tri-phasic slurry batch reactor (Parr 4575, Moline, IL, USA). The reaction mixture was prepared by dissolving ~0.3 g of dibenzothiophene (representing S-bearing species present in oil-derived middle distillates) in 100 cm^3 of *n*-hexadecane (98 mass % and 99+ mass %, respectively, both from Aldrich, Darmstadt, Germany). *N*-hexadecane (cetane) well-represented the hydrocarbons extant in aforementioned real feedstocks from which diesel fuel is produced. Approximately ~0.2 g of sieved sulfided catalyst (80–100 Tyler mesh, ~0.165 mm average particle diameter) were also added, avoiding contact with atmospheric air, precluding sulfates formation. The HDS test reactions were carried out at T = 320 °C, P = 5.67 MPa, and 1000 rpm (~105 rad s^{-1}, mixing speed). Catalysts' particle size and operating conditions were carefully chosen to avoid internal/external diffusional limitations [73]. Liquid samples were taken from the reactor, periodically, then analyzed by gas chromatography (Agilent (Santa Clara, CA, USA) 6890N with flame ionization detector and Econo-Cap-5 capillary column length: 30 m, 0.53 mm diameter, and film thickness of 1.2 μm, from Alltech (Nicholasville, KY, USA). The HDS kinetic constants were calculated assuming pseudo-first order model kinetics referred to DBT concentration and zero order with respect to excess H_2, as follows:

$$k = \frac{-\ln(1-x)}{t_r} \quad (1)$$

where x is DBT conversion and t_r refers to reaction time. The k values for various catalysts were normalized by considering the reaction volume and the mass of the catalyst used (k expressed in m^3 $kg_{cat}{}^{-1}$ s^{-1}). It should be mentioned that H_2S, a byproduct from S-C bond scission reactions, contributed in maintaning tested catalysts in sulfided form and then avoiding their reduction to corresponding metallic phases, characterized by being prone to sintering [74].

4. Conclusions

Alumina-lantana (1, 3, or 5 wt% La) mixed oxides of suitable texture, to be applied as supports of catalysts for hydrotreatment of oil-derived middle-distillates, were prepared by a sol-gel method. In general, the amount and strength of surface basic sites increased with rare-earth content in binary carriers. La at low content (1 wt%) was beneficial in sulfided P-doped CoMo formulations where enhanced dibenzothiophene hydrodesulfurization (HDS) activity (~38%), as to that over the Al_2O_3-supported counterpart, was observed. However, increased La concentration in supports was detrimental on HDS properties. Hardly sulfidable tetrahedral Mo species, originated during impregnation at basic conditions, in pores of La-modified carriers seemed to dictate that behavior. Augmented rare earth concentrations in mixed supports of sulfided CoMo catalysts favored dibenzothiophene conversion through the direct desulfurization (DDS) reaction pathway to biphenyl, over the hydrogenation (HYD) one. That fact, presumably originated in enhanced MoS_2 promotion by efficient Co integration, seems to be promising in the development of alumina-supported HDT formulations at low La content of limited expensive hydrogen consumption.

Supplementary Materials: The following are available online at http://www.mdpi.com/2073-4344/9/4/359/s1, Figure S1: N_2 adsorption isotherms (at −198 °C) of alumina support (A) and La-modified carriers at various rare earth contents (ALaz). Closed symbols: adsorption branch; open symbols: desorption branch. Figure S2: N_2 physisorption isotherms (at −198 °C) of oxidic P-doped CoMo materials impregnated over sol-gel alumina (A) and corresponding La-modified (ALaz) carriers. Closed symbols: adsorption branch; open symbols: desorption branch. Figure S3: Pore size distributions of various prepared supports (a) and oxidic Co-Mo-P impregnated materials (b), as calculated by Barrett-Joyner-Halenda methodology with data from adsorption branch of corresponding N_2 adsorption isotherms. Figure S4: SEM micrographs of La-modified supports. At 1000× magnification, back-scattered electrons detector. (a) ALa1; (b) ALa3; (c) ALa5. Figure S5: SEM micrographs of Co-Mo-P impregnated oxidic samples on alumina and La-modified supports. At 4000× magnification, back-scattered electrons detector. (a) CM/A; (b) CM/ALa1 (c) CM/ALa3; (d) CM/ALa5. Table S1: SEM-EDS chemical analysis of Co-Mo-P impregnated oxidic materials prepared. Scheme S1: Absorption bands in the infrared region of CO_2 species adsorbed on basic sites [from ref. S1]. Scheme S2: Dibenzothiophene HDS reaction network over sulfided $CoMo/Al_2O_3$ [from ref. S2]. HDBT´s: hydrodibenzothiophenes; BP: biphenyl; CHB: cyclohexylbenzene; BCH: bicyclohexyl.

Author Contributions: Funding acquisition, J.E.; Investigation, J.E., M.C.B., J.S.V., D.A.S.-C., V.S., J.E.T., and B.A.R.F.; Project administration, J.E.; Validation, J.E. and M.C.B.; Writing, review and editing, J.E. and M.C.B.

Funding: 117086 SENER-CONACYT-Hidrocarburos grant and Y.00105 Project from IMP.

Acknowledgments: J. Escobar acknowledges financial support from IMP (Y.00105) and SENER-CONACYT-Hidrocarburos (115086) fund.

Conflicts of Interest: The authors declare no conflict of interest.

References

1. Xu, J.; Guo, Y.; Huang, T.; Fan, Y. Hexamethonium bromide-assisted synthesis of CoMo/graphene catalysts for selective hydrodesulfurization. *Appl. Catal. B Environ.* **2019**, *244*, 385–395. [CrossRef]
2. Yang, L.; Peng, C.; Fang, X.; Cheng, Z.; Zhou, Z. Hierarchically macro-mesoporous Ni-Mo/Al_2O_3 catalysts for hydrodesulfurization of dibenzothiophene. *Catal. Commun.* **2019**, *121*, 68–72. [CrossRef]
3. Zhang, C.; Brorson, M.; Li, P.; Liu, X.; Liu, T.; Jiang, Z.; Li, C. CoMo/Al_2O_3 catalysts prepared by tailoring the surface properties of alumina for highly selective hydrodesulfurization of FCC gasoline. *Appl. Catal. A Gen.* **2019**, *570*, 84–95. [CrossRef]
4. Mey, D.; Brunet, S.; Canaff, C.; Maugé, F.; Bouchy, C.; Diehl, F. HDS of a model FCC gasoline over a sulfided CoMo/Al_2O_3 catalyst: Effect of the addition of potassium. *J. Catal.* **2004**, *227*, 436–447. [CrossRef]
5. Klimova, T.; Solís Casados, D.; Ramírez, J. New selective Mo and NiMo HDS catalysts supported on Al_2O_3-MgO(x) mixed oxides. *Catal. Today* **1998**, *43*, 135–146. [CrossRef]
6. Lu, J.; Luo, Y.; He, D.; Xu, Z.; He, S.; Xie, D.; Mei, Y. An exploration into potassium (K) containing MoS_2 active phases and its transformation process over MoS_2 based materials for producing methanethiol. *Catal. Today* **2019**. [CrossRef]
7. Alphonse, P.; Faure, B. Thermal stabilization of alumina modified by lanthanum. *Microporous Mesoporous Mater.* **2014**, *196*, 191–198. [CrossRef]
8. Lu, J.; Hao, H.; Zhang, L.; Xu, Z.; Zhong, L.; Zhao, Y.; He, D.; Liu, J.; Chen, D.; Pu, H.; et al. The investigation of the role of basic lanthanum (La) species on the improvement of catalytic activity and stability of HZSM-5 material for eliminating methanethiol-(CH_3SH). *Appl. Catal. B Environ.* **2018**, *237*, 185–197. [CrossRef]
9. Garbarino, G.; Vijayakumar, R.P.P.; Riani, P.; Finocchio, E.; Busca, G. Ethanol and diethyl ether catalytic conversion over commercial alumina and lanthanum-doped alumina: Reaction paths, catalyst structure and coking. *Appl. Catal. B Environ.* **2018**, *236*, 490–500. [CrossRef]
10. Garbarino, G.; Wang, C.; Valsamakis, I.; Chitsazan, S.; Riani, P.; Finocchio, E.; Flytzani-Stephanopoulos, M.; Busca, G. Acido-basicity of lanthana/alumina catalysts and their activity in ethanol conversion. *Appl. Catal. B Environ.* **2017**, *200*, 458–468. [CrossRef]
11. Garbarino, G.; Wang, C.; Cavattoni, T.; Finocchio, E.; Riani, P.; Flytzani-Stephanopoulos, M.; Busca, G. A study of Ni/La-Al_2O_3 catalysts: A competitive system for CO_2 methanation. *Appl. Catal. B Environ.* **2018**. [CrossRef]
12. He, D.; Zhao, Y.; Yang, S.; Mei, Y.; Yu, J.; Liu, J.; Chen, D.; He, S.; Luo, Y. Enhancement of catalytic performance and resistance to carbonaceous deposit of lanthanum (La) doped HZSM-5 catalysts for decomposition of methyl mercaptan. *Chem. Eng. J.* **2018**, *336*, 579–586. [CrossRef]
13. Cui, J.-W.; Massoth, F.E.; Topsøe, N.Y. Studies of Molybdena-Alumina Catalysts XVIII. Lanthanum-Modified Supports. *J. Catal.* **1992**, *136*, 361–377.
14. Blanchard, P.; Payen, E.; Grimblot, J.; Le Bihan, L.; Poulet, O.; Loutaty, R. Preparation of Co-Mo-based hydrodesulphurization catalysts: Characterizations of deposited species on lanthanum modified γ-alumina. *J. Mol. Catal. A Chem.* **1998**, *135*, 143–153. [CrossRef]
15. Afanasiev, P.; Bezverkhyy, I. Ternary transition metals sulfides in hydrotreating catalysis. *Appl. Catal. A Gen.* **2007**, *322*, 129–141. [CrossRef]
16. Escobar, J.; Barrera, M.C.; Solís-Casados, D.A.; Santes, V.; Sánchez-Valente, J.; Terrazas, J.E. Hidrodesulfuración de dibenzotiofeno sobre CoMo/Al_2O_3-La sol-gel. Effecto del contenido de tierra rara. In Proceedings of the Livro de atas XXVI Congresso Ibero-americano de Catálise (CICAT 2018), Coimbra, Portugal, 9–14 September 2018; Gomes, H., Silva, A., Machado, B., Ribeiro, F., Fonseca, I., Faria, J., Pereira, M., Rocha, R., Eds.; Abstract number: P-IR21. Sociedade Portuguesa de Química: Coimbra, Portugal, 2018; pp. 1070–1075.

17. Leofanti, G.; Padovan, M.; Tozzola, G.; Venturelli, B. Surface area and pore texture of catalysts. *Catal. Today* **1998**, *41*, 207–219. [CrossRef]
18. Dicks, A.L.; Ensell, R.L.; Phillips, T.R.; Szczepura, A.K.; Thorley, M.; Williams, A.; Wragg, R.D. A study of relationships between pore size distribution, hydrogen chemisorption, and activity of hydrodesulphurisation catalysts. *J. Catal.* **1981**, *72*, 266–273. [CrossRef]
19. Gurvich, L. Physico-chemical attractive force. *J. Russ. Phys. Chem. Soc.* **1915**, *47*, 805–827.
20. Ou, E.; Zhou, J.; Mao, S.; Wang, J.; Xia, F.; Min, L. Highly efficient removal of phosphate by lanthanum-doped mesoporous SiO_2. *Colloid Surf. A* **2007**, *308*, 47–53. [CrossRef]
21. Zhang, L.; Wan, L.; Chang, N.; Liu, J.; Duan, C.; Zhou, Q.; Li, X.; Wang, X. Removal of phosphate from water by activated carbon fiber loaded with lanthanum oxide. *J. Hazard. Mater.* **2011**, *190*, 848–855. [CrossRef]
22. Kaluža, L.; Gulková, D.; Vít, Z.; Zdražil, M. High-activity MgO-supported CoMo hydrodesulfurization catalysts prepared by non-aqueous impregnation. *Appl. Catal. B Environ.* **2015**, *162*, 430–436. [CrossRef]
23. Escobar, J.; De Los Reyes, J.A.; Viveros, T. Influence of the Synthesis Additive on the Textural and Structural Characteristics of Sol-Gel Al_2O_3-TiO_2. *Ind. Eng. Chem. Res.* **2000**, *39*, 666–672. [CrossRef]
24. Chaturvedi, S.; Dave, P.N. Review on Thermal Decomposition of Ammonium Nitrate. *J. Energ. Mater.* **2013**, *31*, 1–26. [CrossRef]
25. Barrera, A.; Fuentes, S.; Viniegra, M.; Avalos-Borja, M.; Bogdanchikova, N.; Campa-Molina, J. Structural properties of Al_2O_3-La_2O_3 binary oxides prepared by sol-gel. *Mater. Res. Bull.* **2007**, *42*, 640–648. [CrossRef]
26. Escobar, J.; Barrera, M.C.; De Los Reyes, J.A.; Cortés, M.A.; Santes, V.; Gómez, E.; Pacheco, J.G. Effect of Mo and Co loading in HDS catalysts supported on solvo-thermally treated ZrO_2-TiO_2 mixed oxide. *Catal. Today* **2008**, *133–135*, 282–291. [CrossRef]
27. Hattori, H. Heterogeneous Basic Catalysis. *Chem. Rev.* **1995**, *95*, 537–558. [CrossRef]
28. Bálsamo, N.; Mendieta, S.; Heredia, A.; Crivello, M. Nanoclays as dispersing precursors of La and Ce oxide catalysts to produce high-valued derivatives of biodiesel by-product. *Mol. Catal.* **2019**. [CrossRef]
29. Bernal, S.; Díaz, J.A.; García, J.R.; Rodríguez-Izquierdo, J.M. Study of some aspects of the reactivity of La_2O_3 with CO_2 and H_2O. *J. Mater. Sci.* **1985**, *20*, 537–541. [CrossRef]
30. Morterra, C.; Ghiotti, G.; Boccuzzi, F.; Coluccia, S. An infrared spectroscopic investigation of the surface properties of magnesium aluminate spinel. *J. Catal.* **1978**, *51*, 299–313. [CrossRef]
31. Di Cosimo, J.I.; Diez, V.K.; Xu, M.; Iglesia, E.; Apesteguia, C.R. Structure and Surface and Catalytic Properties of Mg-Al Basic Oxides. *J. Catal.* **1998**, *78*, 499–510. [CrossRef]
32. Boukha, Z.; Fitian, L.; López-Haro, M.; Mora, M.; Ruiz, J.R.; Jiménez-Sanchidrián, C.; Blanco, G.; Calvino, J.J.; Cifredo, G.A.; Trasobares, S.; et al. Influence of the calcination temperature on the nano-structural properties, surface basicity, and catalytic behavior of alumina-supported lanthana samples. *J. Catal.* **2010**, *272*, 121–130. [CrossRef]
33. Bettman, M.; Chase, R.E.; Otto, K.; Weber, W.H. Dispersion Studies on the System La_2O_3/γ-$A1_2O_3$. *J. Catal.* **1989**, *117*, 447–454. [CrossRef]
34. Kraus, H.; Prins, R. Proton NMR Investigations of Surface Hydroxyl Groups on Oxidic Mo-P/γ-Al_2O_3 Catalysts. *J. Catal.* **1996**, *164*, 260–267. [CrossRef]
35. Ledford, J.S.; Kim, Y.-M.; Houalla, M.; Proctor, A.; Hercules, D.M. Surface Analysis of Lanthanum-modified Cobalt Catalysts. *Analyst* **1992**, *117*, 323–327. [CrossRef]
36. Wachs, I.E. Raman and IR studies of surface metal oxide species on oxide supports: Supported metal oxide catalysts. *Catal. Today* **1996**, *27*, 437–455. [CrossRef]
37. Scheithauer, M.; Knözinger, H.; Vannice, M.A. Raman Spectra of La_2O_3 Dispersed on γ-Al_2O_3. *J. Catal.* **1998**, *178*, 701–7005. [CrossRef]
38. Dedov, A.G.; Loktev, A.S.; Moiseev, I.I.; Aboukais, A.; Lamonier, J.F.; Filimonov, I.N. Oxidative coupling of methane catalyzed by rare earth oxides: Unexpected synergistic effect of the oxide mixtures. *Appl. Catal. A Gen.* **2003**, *245*, 209–220. [CrossRef]
39. Chen, J.; Mi, J.; Li, K.; Wang, X.; Dominguez Garcia, E.; Cao, Y.; Jiang, L.; Oliviero, L.; Mauge, F. The role of citric acid in preparing highly active CoMo/Al_2O_3 catalyst: From aqueous impregnation solution to active site formation. *Ind. Eng. Chem. Res.* **2017**, *56*, 14172–14181. [CrossRef]
40. Nicosia, D.; Prins, R. ^{31}P MAS NMR and Raman study of a Co(Zn)MoP/γ-Al_2O_3 HDS catalyst precursor containing triethylene glycol. *J. Catal.* **2005**, *234*, 414–420. [CrossRef]

41. Bergwerff, J.A.; Visser, T.; Leliveld, B.R.G.; Rossenaar, B.D.; de Jong, K.P.; Weckhuysen, B.M. Envisaging the physicochemical processes during the preparation of supported catalysts: Raman microscopy on the impregnation of Mo onto Al_2O_3 extrudates. *J. Am. Chem. Soc.* **2004**, *126*, 14548–14556. [CrossRef]
42. Catita, L.; Quoineaud, A.-A.; Espinat, D.; Pichon, C.; Delpoux, O. Application of magnetic resonance imaging and raman imaging to study the impact of phosphorus in impregnation of hydrotreatment catalysts. *Appl. Catal. A Gen.* **2017**, *547*, 164–175. [CrossRef]
43. Kraus, H.; Prins, R. Composition of impregnation solutions and wet impregnated Mo-P/γ-Al_2O_3 catalysts as investigated by ^{31}P and ^{95}Mo NMR. *J. Catal.* **1995**, *164*, 251–259. [CrossRef]
44. Vázquez-Garrido, I.; López-Benítez, A.; Berhault, G.; Guevara-Lara, A. Effect of support on the acidity of NiMo/Al_2O_3-MgO and NiMo/TiO_2-Al_2O_3 catalysts and on the resulting competitive hydrodesulfurization/hydrodenitrogenation reactions. *Fuel* **2019**, *236*, 55–64. [CrossRef]
45. Ishutenko, D.; Nikulshin, P.; Pimerzin, A. Relation between composition and morphology of K(Co)MoS active phase species and their performances in hydrotreating of model FCC gasoline. *Catal. Today* **2016**, *271*, 16–27. [CrossRef]
46. Solís-Casados, D.A.; Escobar-Alarcón, L.; Klimova, T.; Escobar-Aguilar, J.; Rodríguez-Castellón, E.; Cecilia, J.A.; Morales-Ramírez, C. Catalytic performance of CoMo/Al_2O_3-MgO-Li(x) formulations in DBT hydrodesulfurization. *Catal. Today* **2016**, *271*, 35–44. [CrossRef]
47. Sheik Saleem, S.; Aruldhas, G. Raman and Infrared Spectra of Lanthanum Molybdate. *J. Solid State Chem.* **1982**, *42*, 158–162. [CrossRef]
48. Frank, C.J.; Redd, D.C.B.; Gansler, T.S.; McCreery, R.L. Characterization of Human Breast Biopsy with Near-IR Raman Spectroscopy Specimens. *Anal. Chem.* **1994**, *66*, 319–326. [CrossRef]
49. Ramírez, J.; Macías, G.; Cedeño, L.; Gutiérrez-Alejandre, A.; Cuevas, R.; Castillo, P. The role of titania in supported Mo, CoMo, NiMo, and NiW hydrodesulfurization catalysts: Analysis of past and new evidences. *Catal. Today* **2004**, *98*, 19–30. [CrossRef]
50. Liu, Y.; Liu, X.; Zhao, L.; Lyu, Y.; Xu, L.; Rood, M.J.; Wei, L.; Liu, Z.; Yan, Z. Effect of lanthanum species on the physicochemical properties of La/SAPO-11 molecular sieve. *J. Catal.* **2017**, *347*, 170–184. [CrossRef]
51. Torres-Mancera, P.; Ramírez, J.; Cuevas, R.; Gutiérrez-Alejandre, A.; Murrieta, F.; Luna, R. Hydrodesulfurization of 4,6-DMDBT on NiMo and CoMo catalysts supported on B_2O_3-Al_2O_3. *Catal. Today* **2005**, *107–108*, 551–558. [CrossRef]
52. Weber, R.S. Effect of local structure on the UV-visible absorption edges of molybdenum oxide clusters and supported molybdenum oxides. *J. Catal.* **1995**, *151*, 470–474. [CrossRef]
53. Sreedhara, M.B.; Ramakrishna Matte, H.S.S.; Govindaraj, A.; Rao, C.N.R. Synthesis, Characterization, and Properties of Few-Layer MoO_3. *Chem. Asian J.* **2013**, *8*, 2430–2435. [CrossRef] [PubMed]
54. Makshina, E.V.; Zhilinskaya, E.A.; Siffert, S.; Mazo, G.N.; Aboukaïs, A.; Grünert, W.; Romanovsky, B.V. Nanostructured lanthanum cobaltate: Oxidation and coordination states of Co atoms. *J. Exp. Nanosci.* **2009**, *5*, 427–437. [CrossRef]
55. Xie, L.L.; Gao, Q.M.; Li, Q.H. Nanoporous metal phosphate CoVSB-1 catalyst for oxidation of styrene with H_2O_2. In *From Zeolites to Porous MOF Materials—The 40th Anniversary of International Zeolite Conference. Proceedings of the 15th International Zeolite Conference, Beijing, China, 12–17 August 2007*; Xu, R., Gao, Z., Chen, J., Yan, W., Eds.; Elsevier B.V.: Amsterdam, The Netherlands, 2007; pp. 1338–1343.
56. Martin, C.; Martin, I.; Rives, V.; Malet, P. Changes in the Struture of TiO_2-supported Molybdena Induced by Na-doping. *J. Catal.* **1994**, *147*, 465–475. [CrossRef]
57. Topsøe, N.Y.; Topsøe, H. FTIR Studies of Mo/Al_2O_3-Based Catalysts: II. Evidence for the Presence of SH Groups and Their Role in Acidity and Activity. *J. Catal.* **1993**, *139*, 641–651. [CrossRef]
58. Morales, A.; Ramírez de Agudelo, M.M. Promoter Role of Octahedral Co (and Ni) in Modified Co(Ni)Mo-Al_2O_3 Catalysts for Hydrodesulfurization Reactions. *Appl. Catal.* **1986**, *23*, 23–34. [CrossRef]
59. Solís-Casados, D.; Escobar, J.; García Orozco, I.; Klimova, T. Effect of Potassium Content on the Performance of CoMo/Al_2O_3-MgOK_2O(x) Catalysts in Hydrodesulfurization of Dibenzothiophene. *Ind. Eng. Chem. Res.* **2011**, *50*, 2755–2761. [CrossRef]
60. Wu, L.; Jiao, D.; Wang, J.; Chen, L.; Cao, F. The role of MgO in the formation of surface active phases of CoMo/Al_2O_3-MgO catalysts for hydrodesulfurization of dibenzothiophene. *Catal. Commun.* **2009**, *11*, 302–305. [CrossRef]

61. Ge, T.; Zuo, C.; Chen, H.; Muhammad, Y.; Wei, L.; Li, C. Catalytic Activity and Molecular Behavior of Lanthanum Modified CoS_x/γ-Al_2O_3 Catalysts for the Reduction of SO_2 to Sulfur in Smelter Off-Gas Using CO-H_2 Mixture as Reductant. *Ind. Eng. Chem. Res.* **2019**. [CrossRef]
62. Escobar, J.; Barrera, M.C.; Santes, V.; Terrazas, J.E. Naphthalene hydrogenation over Mg-doped Pt/Al_2O_3. *Catal. Today* **2017**, *296*, 197–204. [CrossRef]
63. Houalla, M.; Nag, N.K.; Sapre, A.V.; Broderick, D.H.; Gates, B.C. Hydrodesulfurization of dibenzothiophene catalyzed by sulfided CoO-MoO_3/γ-Al_2O_3: The reaction network. *AIChEJ* **1978**, *24*, 1015–1021. [CrossRef]
64. Hensen, E.J.M.; Kooyman, P.J.; van der Meer, Y.; van der Kraan, A.M.; de Beer, V.H.J.; van Veen, J.A.R.; van Santen, R.A. The relation between morphology and hydrotreating activity for supported MoS_2 particles. *J. Catal.* **2001**, *199*, 224–235. [CrossRef]
65. Bataille, F.; Lemberton, J.L.; Michaud, P.; Pérot, G.; Vrinat, M.; Lemaire, M.; Schulz, E.; Breysse, M.; Kasztelan, S. Alkyldibenzothiophenes hydrodesulfurization-promoter effect, reactivity, and reaction mechanism. *J. Catal.* **2000**, *191*, 409–422. [CrossRef]
66. Wu, Z.; Whiffen, V.M.L.; Zhu, W.; Wang, D.; Smith, K.J. Effect of Annealing Temperature on Co-MoS_2 Nanosheets for Hydrodesulfurization of Dibenzothiophene. *Catal. Lett.* **2014**, *144*, 261–267. [CrossRef]
67. Kaluža, L.; Gulková, D.; Vít, Z.; Zdražil, M. Effect of support type on the magnitude of synergism and promotion in CoMo sulphide hydrodesulphurisation catalyst. *Appl. Catal. A Gen.* **2007**, *324*, 30–35. [CrossRef]
68. Wu, H.; Duan, A.; Zhao, Z.; Qi, D.; Li, J.; Liu, B.; Jiang, G.; Liu, J.; Wei, Y.; Zhang, X. Preparation of NiMo/KIT-6 hydrodesulfurization catalysts with tunable sulfidation and dispersion degrees of active phase by addition of citric acid as chelating agent. *Fuel* **2014**, *130*, 203–210. [CrossRef]
69. Halachev, T.; Atanasova, P.; Lopez Agudo, A.; Arias, M.G.; Ramirez, J. Activity of P-Ni-W/Al_2O_3 catalysts with varying phosphorus content in the hydrogenation of naphthalene. *Appl. Catal. A Gen.* **1996**, *136*, 161–175. [CrossRef]
70. Wang, T.; Fan, Y.; Wang, X.; Chou, L.; Lin, H. Selectivity enhancement of CoMoS catalysts supported on tri-modal porous Al_2O_3 for the hydrodesulfurization of fluid catalytic cracking gasoline. *Fuel* **2015**, *157*, 171–176. [CrossRef]
71. Jaf, Z.N.; Altarawneha, M.; Miran, H.A.; Jiang, Z.T.; Dlugogorski, B.Z. Hydrodesulfurization of Thiophene over γ-Mo_2N catalyst. *Mol. Catal.* **2018**, *459*, 21–30. [CrossRef]
72. Fujikawa, T.; Chiyoda, O.; Tsukagoshi, M.; Idei, K.; Takehara, S. Development of a high activity HDS catalyst for diesel fuel: From basic research to commercial experience. *Catal. Today* **1998**, *45*, 307–312. [CrossRef]
73. Escobar, J.; Gutiérrez, A.; Barrera, M.C.; Colín, J.A. NiMo/alumina hydrodesulphurization catalyst modified by saccharose: Effect of addition stage of organic modifier. *Can. J. Chem. Eng.* **2016**, *94*, 66–74. [CrossRef]
74. Shalagina, A.E.; Aleshina, G.I.; Startsev, A.N. Hydrogen occluded in sulfide catalysts: Evidence from the temperature programmed heating Technique. *React. Kinet. Catal. Lett.* **2003**, *78*, 91–98. [CrossRef]